ACS Macro Letters

Letter

pubs.acs.org/macroletters

Mitigating the Cytotoxicity of Graphene Quantum Dots and Enhancing Their Applications in Bioimaging and Drug Delivery

Anil Chandra,[†,‡,§] Sonal Deshpande,[†,‡,§] Dhanraj B. Shinde,[∥] Vijayamohanan K. Pillai,[⊥] and Neetu Singh*[,†,‡]

[†]Centre for Biomedical Engineering, Indian Institute of Technology Delhi, Hauz Khas, New Delhi 110016, India

[‡]Division of Polymer Science and Engineering, National Chemical Laboratory, Dr. Homi Bhaba Road, Pune 411008, India

[∥]Physical and Materials Chemistry Division, National Chemical Laboratory, Pune 411008, India

[⊥]Central Electrochemical Research Institute, College Road, Karaikudi, Tamil Nadu 630006, India

Supporting Information

ABSTRACT: Despite the promising photophysical properties of fluorescent graphene quantum dots (GQDs), their cellular toxicity needs to be addressed before their full potential could be completely realized in biomedicine. A simple method for mitigating the toxicity of GQDs by embedding them in PEG matrix is reported here. The enhanced biocompatibility of polymer modified, P-GQDs, is attributed to reduced reactive oxygen species generation, as measured by an intracellular ROS assay. We also demonstrate the enhanced loading and efficient intracellular delivery of therapeutics by P-GQDs.

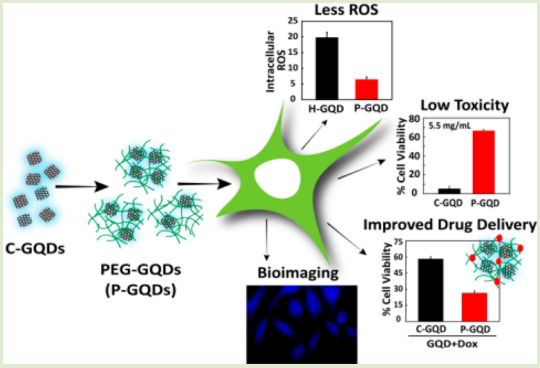

Graphene quantum dots (GQDs) are emerging as promising materials for biomedical applications.[1−5] They are being extensively investigated for cellular imaging and drug delivery due to their high intrinsic fluorescence and large surface area with delocalized electrons, suitable for loading drugs using $\pi-\pi$ interactions.[1,6−8] In recent times, GQDs have gathered huge interest since they are "all carbon" material and unlike inorganic quantum dots their degradation may not result in any toxic metal ions. Additionally, their stable photoluminescence, unique excitation dependent emission, solubility in variety of solvents, chemical inertness, native functional groups at the edges, and easy tunability of size and shape makes them extremely attractive for biomedical applications.[3] Recently it was shown that GQDs can deliver a chemotherapeutic selectively to the cell nucleus and can also enhance DNA cleavage activity of the drug, thus, improving its efficacy.[7] Despite such applications, the cytotoxicity of the GQDs is a major concern for further development of the field.[1,9−11] The toxicity of graphene oxides to macrophages and its hemolytic properties has been recently reported.[10,12]

Many reports show that GQDs can be well tolerated up to a certain concentration, though the concentrations seem fairly low for many practical bioapplications. For instance, 100% cell viability with GQDs was observed only at concentrations <50 μg/mL and almost 50% cells were found dead at concentrations around 1 mg/mL.[9,13−15] Recently, polymer coating of the GQDs resulting into a thin shell was employed, still significant toxicity was observed even with the polymer coated GQDs.[16,17] Thus, despite several efforts for improving their biocompatibility, the cytotoxicity observed is an issue that needs to be resolved before realizing larger biomedical applications of GQDs. Also, the drug delivery capabilities of GQDs have been limited as only the adsorption of drugs on the GQDs has been employed until date.[18,19]

In order to mitigate the cytotoxicity of GQDs, we worked with two current hypotheses. It is believed that the toxicity of GQDs may be due to their size; small-sized GQDs (<10 nm) can have catalytically active surfaces, sharp edges, and can penetrate the nucleus causing severe cellular damage.[7,11,20] Increasing the size of GQDs, while a potential solution, unfortunately decreases its luminescence properties.[21,22] A second cause for toxicity at higher concentrations (~100 μg/mL) is believed to be the ability of GQDs to generate more reactive oxygen species (ROS) intracellularly.[9,23] Polymer, especially polyethylene glycol (PEG) shells has been used in the literature to decrease the toxicity of GQDs, nevertheless, even after polymer coating the cell viability at higher concentrations (above 1 mg/mL) was found to be low.[6,16] It is possible that even though the ROS production can be lowered by the polymer shell coating, the size of the GQDs after coating remains small (sub 50 nm) and are still in the size

Received: August 6, 2014
Accepted: October 2, 2014
Published: October 6, 2014

range that can interact with intracellular proteins and organelles.

Encouraged by these hypotheses and proof-of-concept demonstrations, here we have employed a new approach that addresses both sources of toxicity and there by achieved the lowest reported cytotoxicity. Whereas a polymer coating does not increase size dramatically, we embedded the GQDs in a PEG matrix instead of coating the polymer on the surface (Scheme 1), thus, yielding bigger (>100 nm) nanoparticles.

Scheme 1. Schematic for the Synthesis of Biocompatible GQDs

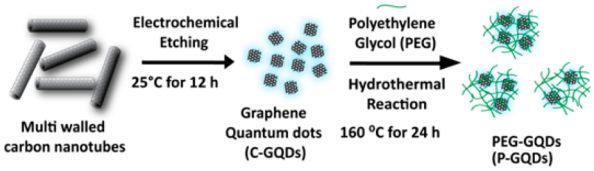

This strategy allows confinement of the small GQDs inside a larger biocompatible matrix, dramatically reducing their ability to interact with cellular organelles. The PEG matrix can also help in reducing intracellular ROS.[10] We demonstrate that the encapsulated GQDs (P-GQDs) indeed show reduced ROS production, shutting off one major source of toxicity. The P-GQD nanoparticles were internalized by HeLa cells and serve as cellular imaging probes. Finally, we investigated if the PEG network can be utilized for loading and delivering chemotherapeutics to cells.

We synthesized GQDs by electrochemical unzipping of multiwalled carbon nanotubes (MWCNTs) as per a slightly modified recently reported method.[24] This simple electrochemical procedure provides good control over size and shape of the GQDs and yields GQDs without any toxic byproducts. Briefly, the synthesis was carried at room temperature by application of an interfacial electric field for oxidation followed by reduction of the MWCNTs. The water-soluble crude-GQDs (C-GQDs), thus obtained, were PEGylated to form PEG nanoparticles with GQDs embedded in them (P-GQDs). The PEGylation was performed using a previously reported hydrothermal method.[25] We first optimized the concentration of PEG to yield ∼100 nm matrix rather than coating single GQDs with a shell, which would yield <40 nm particles. At a higher concentration of PEG, large ∼80−100 nm spherical particles were observed due to the hydrothermal polymerization,[26,27] as indicated by the changes in CH_2 to OH peaks in NMR (Figure S1), whereas, at lower concentrations such big polymeric assemblies were not observed (Figure S2a,S2b and S2c). The variation in concentration was used to obtain GQDs with either a PEG shell (S-GQDs) or embedded in a PEG matrix (P-GQDs; Figure S3). The hydrothermal reaction of GQDs with PEG (MW 8 kDa) was carried out at 160 °C in an autoclave. After 24 h, the solution obtained was dialyzed to remove unreacted PEG, yielding P-GQDs. A similar hydrothermal protocol was followed without PEG to obtain hydrothermally treated-GQDs (H-GQDs), which were used as control sample for studying the effect of hydrothermal treatment on GQDs. For investigating the effect of embedding GQDs into PEG matrix in comparison to coating with a polymer shell, we synthesized S-GQDs, GQDs with a PEG shell, via a similar hydrothermal treatment but with less concentration of PEG.

We characterized the PEGylation of GQDs by Fourier transform infrared spectroscopy (FTIR). The FTIR spectra for C-GQDs, free PEG, H-GQDs, and P-GQDs are shown in Figure S4a. The C-GQDs and H-GQDs both showed the presence of alkane C−H, C═C, and O−H vibrations. The P-GQDs showed the presence of both PEG and GQD signature peaks at 2880 and 1640 cm^{-1}.[25] In addition, the P-GQDs also show peaks around 2950 and 3460 cm^{-1} corresponding to the C−H stretch from GQDs and O−H stretch from the PEG, respectively. We also confirmed PEGylation by X-ray photoelectron spectroscopy (XPS) of the C1s level in GQD samples before and after PEGylation (Figure S5). The C−C (284.4 eV), C−OH (285.7 eV), and C−O (286.6 eV) binding energy peaks were observed in all the samples. However, the C−OH (285.7 eV) peak was significantly higher for P-GQDs as compared to C-GQDs and H-GQDs, as attributable to some unreacted −OH groups from PEG and hydroxyl groups from the GQD surface. The hydrothermal process is known to reduce oxygenated functional groups, such as carboxylic acid, epoxy, alkoxy, and carbonyl present on the C-GQD surface to hydroxyl.[22] This was indicated by the loss of C═O (288.5 eV) and C−O−C (287.2 eV) peaks in H-GQD compared to C-GQDs.

The morphology and size of the GQDs were characterized by transmission electron microscopy (TEM) and atomic force microscopy (AFM). The average diameter of C-GQDs was found to be 6.6 ± 0.7 nm, indicating a narrow dispersion (Figures 1 and S6a). The topographic height was observed to

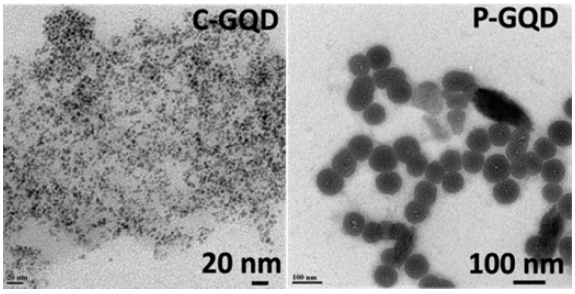

Figure 1. TEM images for C-GQDs and P-GQD.

be ∼1−2 nm (Figure S6e). The hydrothermal treatment does not aggregate or change the size of the GQDs (Figure S6b): the average size of H-GQDs was similar to C-GQDs. The PEGylation process yielded 88 ± 18 nm nanoparticles consisting of individual GQDs embedded in a PEG matrix (Figures 1, S6c, and S6d). The size of GQDs inside the PEG matrix remained unaltered (Figure S6d), indicating no adverse effect of the PEGylation process on GQD size. A lower concentration of PEG resulted in smaller-sized nanoparticles (38 ± 6 nm), S-GQDs, which are GQDs coated with a PEG shell (Figure S3b).

Since the PEGylation process did not affect the size of individual GQDs, we hypothesized that the size-dependent optical properties of GQDs should be maintained. As confirmation, we performed UV−vis absorption and Photoluminescence (PL) measurements. The quantum yield of the GQDs was estimated to be ∼3−4%, which is comparable to graphene based bioimaging probes used in the literature.[28] Interestingly, the hydrothermal treatment and PEGylation process did not affect the quantum yield (Table S1). The UV−vis absorption spectra of C-GQDs, H-GQDs, S-GQDs,

dx.doi.org/10.1021/mz500479k | ACS Macro Lett. 2014, 3, 1064−1068

and P-GQDs were similar to a broad absorption band at ~270 nm (Figures S3 and S7a). The PL spectrum (Figures S3, S4b, and S7b) for C-GQDs, H-GQDs, S-GQDs, and P-GQDs showed the characteristic excitation-dependent PL behavior of GQDs with a broad peak around 420 nm.[22,24,29] Photoluminescence excitation (PLE) spectra for GQDs before and after PEGylation were also similar, with two distinct peaks at 240 and 330 nm. Thus, we confirmed that the PEGylation does not adversely affect the optical properties of GQDs, making them useful for bioimaging.

We first assessed the effect of PEGylation on nonspecific protein interaction of GQDs via a protein-GQD interaction assay (Figure S8a). We incubated the C-GQDs, H-GQDs, S-GQDs, and P-GQDs with BSA solution at 37 °C for 2 h. After the interaction with proteins the aggregated GQD-protein can be pelleted out easily by centrifugation. The samples were thus centrifuged and the pellet and supernatant ran over a gel to analyze the presence of proteins. As can be seen from Figures S8b and S8c, P-GQDs had the least interaction with the protein as indicated by less protein in the pellet and more protein in the supernatant. S-GQDs also showed less protein in the pellet compared to C-GQDs and H-GQDs, confirming the ability of PEG to resist protein interaction. On the other hand, for C-GQDs and H-GQDs, more protein was observed in the pellet, compared to the supernatant (Figure S8b). These results confirmed our hypothesis that smaller-sized GQDs without PEG interacted with proteins the most, followed by smaller-sized, PEG-coated GQDs (S-GQDs), compared to the GQDs embedded in PEG matrix.

Next, we assessed the cytotoxicity of GQDs via (3-(4,5-dimethylthiazol-2-yl)-2,5-diphenyltetrazolium bromide (MTT) assay, which is a colorimetric assay for quantifying cell viability. HeLa cells were incubated with various concentrations of C-GQDs, H-GQDs, S-GQDs, and P-GQDs for 24 h, after which the cytotoxicity was quantified by dissolving the formazan crystals formed by the live cells and measuring the absorbance at 550 nm. No significant toxicity was observed at GQD concentrations lower than 0.4 mg/mL. At concentrations higher than 0.4 mg/mL, C-GQDs and H-GQDs showed more toxicity than P-GQDs (Figure 2a). The P-GQDs did not show any significant cellular toxicity. At about 4 mg/mL, almost 75% cells were viable for P-GQDs, whereas only 25 and 5% cells were viable for C-GQDs and H-GQDs, respectively. This data suggests that indeed the PEGylation process has made the GQDs less cytotoxic. The excellent cell viability due to P-GQDs was maintained even at a very high concentration. About 50% cells were found viable at ~8 mg/mL. This low cytotoxicity at such high concentrations has not been reported until date. Interestingly, when compared with S-GQDs, P-GQDs were well tolerated even at 4× higher concentration (Figures 2a and S9). S-GQDs showed about 70 and 20% cell viability at 2 and 4 mg/mL, respectively. Thus, confirming our hypothesis that embedding the GQDs in a matrix might reduce the cytotoxicity.

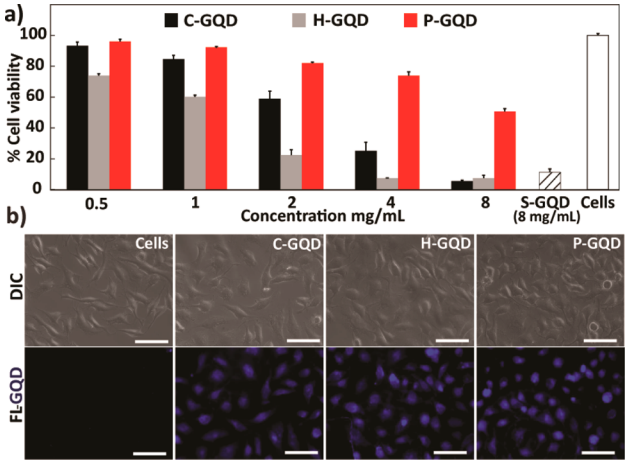

Figure 2. (a) Cell viability for C-GQD, H-GQD, and P-GQDs, as assessed by MTT. Controls: S-GQD (8 mg/mL); Only cells. (b) Cellular labeling of HeLa cells with GQDs. Blue: GQDs. Scale bar is 50 μm.

After confirming the improved biocompatibility of P-GQDs *vis a vis* unmodified GQDs, we evaluated its potential application in bioimaging. We incubated HeLa cells with C-GQDs, H-GQDs, and P-GQDs. As can be seen from fluorescence microscopy images (Figure 2b), all GQDs, including P-GQDs, were easily internalized into the cells after 4 h of incubation. A strong blue fluorescence from the cell cytoplasm was observed for cells incubated with GQDs, compared to the cells without any GQDs. Thus, the cytotoxicity data and uptake experiment together indicate that P-GQDs can be used for cell imaging without adverse cytotoxic effects at higher concentrations (above 1 mg/mL), unlike unmodified GQDs, which are relatively toxic at those concentrations.

We next focused our efforts on investigating the underlying reasons for the observed exceptional biocompatibility of P-GQDs. The cytotoxicity of GQDs at higher concentration is usually attributed to its ability to generate intracellular reactive oxygen species (ROS).[9,23] Recently it has also been reported that GQDs, due to their aromatic sp^2 carbon clusters, have an intrinsic peroxidase-like catalytic activity.[30−32] This property might catalyze intracellular ROS production, usually generated as a byproduct in the normal aerobic cellular metabolism, and may be the source of toxicity for unmodified GQDs. The PEG matrix in close proximity to GQD's surface can act as an ROS scavenger; hence, P-GQDs may be less cytotoxic.[10] Motivated by this hypothesis, we investigated if the toxicity observed at higher concentrations can be correlated to the ROS generating ability of GQDs.

We first studied if the GQDs have any catalytic effect on ROS production in cell-free environment. We incubated the samples (C-GQDs, H-GQDs, S-GQDs, and P-GQDs) with H_2O_2 in 10% fetal bovine serum (FBS) solution at 37 °C. Chemically hydrolyzed 2,7-dichlorodihydrofluorescein diacetate (H_2DCF-DA), yielding H_2DCF, was used as a fluorescent indicator of ROS production.[33] We monitored the increase in ROS over 90 min with 10 μM and 20 μM H_2O_2 in the presence and absence of GQDs. In the case of C-GQDs and H-GQDs incubated with 20 μM H_2O_2, the ROS production increased ~3× and ~4×, respectively (Figure 3a). This was in contrast to P-GQDs, where there was no significant increase in ROS over 90 min. For a lower concentration of H_2O_2 (10 μM), there was no increase in ROS when incubated with P-GQDs (Figure S10). Interestingly, the ROS levels were comparable to samples where no H_2O_2 was added, indicating that the PEG matrix was able to quench even the ROS produced by H_2O_2. A similar but less pronounced quenching was observed for the S-GQDs (Figure S11a). Thus, confirming again the ROS quenching ability of PEG. However, adding free PEG to C-GQDs did not quench the ROS produced in solution (Figure S11b).

dx.doi.org/10.1021/mz500479k | *ACS Macro Lett.* 2014, 3, 1064−1068

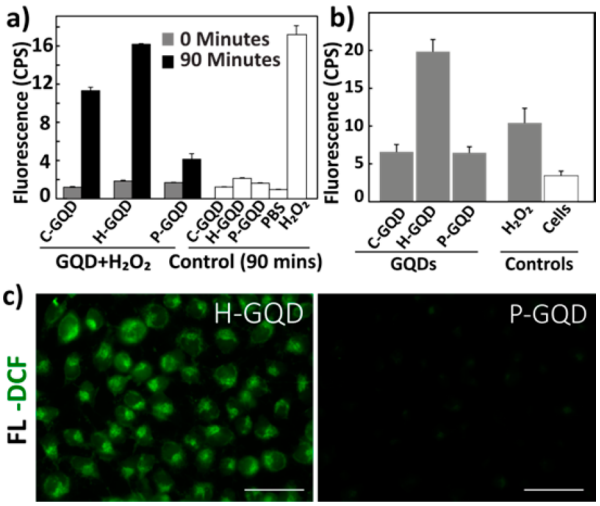

Figure 3. (a) ROS production in solution containing samples with 20 μM H_2O_2 at 0 and 90 min. (b) Intracellular ROS in HeLa cells. (c) Intracellular ROS imaged in HeLa cells. Green: DCF. Scale bar is 50 μm.

Interestingly, more quenching was observed in P-GQDs compared to the S-GQDs, suggesting the ability of a thicker PEG matrix to quench ROS more effectively. C-GQDs and H-GQDs with 10 μM H_2O_2 showed significantly higher ROS production (Figure S10). The H-GQDs produced more ROS than C-GQDs, likely because of more free-radical-susceptible hydroxyl groups on the surface generated by the hydrothermal treatment.

Next, we examined intracellular ROS produced when HeLa cells are incubated with GQDs. HeLa cells were first incubated with 15 μM H_2DCF-DA dye for 1 h followed by incubation with 2 mg/mL GQDs for 6 h. The acetate groups on the nonfluorescent H_2DCF-DA are cleaved by intracellular esterases and further oxidation due to ROS converts H_2DCF to a highly fluorescent 2,7-dichlorofluorescein (DCF). Measurement and visualization of the DCF fluorescence can thus quantify the intracellular ROS production.[9,23] As can be seen from Figures 3b and S12, P-GQDs showed lower intracellular ROS levels compared to H-GQDs, which showed the highest levels of ROS. We also visualized the intracellular ROS produced by the GQDs by imaging cells incubated with dye and GQDs. The cells incubated with H-GQDs showed highest green fluorescence due to ROS formation. The C-GQDs showed little green fluorescence (Figures S12a and S12b), suggesting low but slightly more ROS production compared to cells without any GQDs. On the other hand, P-GQDs showed almost no fluorescence (Figures 3c and S12). Thus, both quantitative fluorescence measurement as well as cell imaging showed less ROS production for P-GQDs as compared to H-GQDs. This emphasizes the ability of PEG matrix to lower the intracellular ROS production usually observed when cells are treated with GQDs. These results indicate the role of ROS production in the high toxicity exhibited by H-GQDs and also the ability of PEG matrix to mitigate this ROS-caused toxicity.

Encouraged by the excellent biocompatibility of P-GQDs, we explored if the PEG matrix can be used to deliver chemotherapeutics. This will allow development of modalities that can be used for imaging as well as therapy. Unmodified GQDs have been demonstrated to deliver chemotherapeutics by loading the drug using $\pi-\pi$ interactions on the GQD surface.[6,7] However, high doses of drug cannot be delivered, as high concentrations of GQDs traditionally result in strong cytotoxicity. We hypothesized high doses might be delivered safely by P-GQDs, as it can be tolerated at significantly higher concentrations. In addition, the PEG matrix can load more drug than the unmodified GQD surface.

We assessed the drug delivery capability of P-GQDs in comparison with unmodified GQDs. For drug loading, C-GQDs and P-GQDs were lyophilized and soaked in doxorubicin (Dox), a chemotherapeutic, solution for 30 min, followed by purification by dialysis. The Dox loading was estimated by measuring the Dox absorbance. For P-GQDs, about twice the amount of Dox was loaded compared to C-GQDs (Figure 4a).The fluorescence of GQDs was also

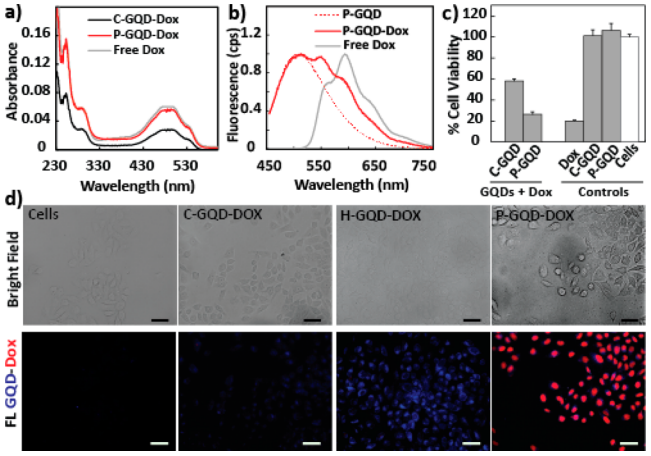

Figure 4. (a) Absorbance spectra and (b) fluorescence spectra, of P-GQD-Dox, C-GQD-Dox, and free Dox. (c) HeLa cell viability after incubation with P-GQD-Dox and C-GQD-Dox. (d) Intracellular delivery of Dox with P-GQD-Dox; red: Dox, blue: GQDs. Scale bar is 50 μm.

unaffected by Dox loading as indicated by the spectra in Figure 4b, where fluorescence due to both GQDs and Dox can be observed in P-GQD-Dox. To test cytotoxic effect of Dox-loaded GQD, we incubated 4 μg/mL C-GQD-Dox and P-GQD-Dox, containing 0.1 and 0.2 μM Dox, respectively, with HeLa cells. Consequently, we assessed the cell viability after 48 h using the MTT assay. For P-GQD-Dox, cell viability was around 26%, whereas for C-GQD-Dox it was ~58% (Figure 4c). More significantly, no toxicity was observed in C-GQDs and P-GQDs without Dox. These results clearly indicate the remarkable ability of P-GQDs to load more Dox and efficiently deliver it in HeLa cells. We also used Dox and GQD fluorescence for imaging the cells after the GQDs were internalized. Accordingly, Figure 4d shows images of HeLa cells incubated with C-GQD-Dox, H-GQD-Dox, and P-GQD-Dox. All GQD samples showed strong blue fluorescence in the cytoplasm of the cells compared to control cells (without GQDs). However, only the P-GQD-Dox had both red and blue fluorescence due to Dox and GQDs, respectively. The Dox appeared to be localized in the nucleus of the cells, whereas GQDs were present in the cytoplasm (Figure S13). These results demonstrate that the P-GQDs can deliver Dox at higher concentrations as compared to C-GQDs. Thus, P-GQDs can provide a platform for delivering chemotherapeutics more efficiently along with enabling intracellular imaging.

dx.doi.org/10.1021/mz500479k | ACS Macro Lett. 2014, 3, 1064−1068

In conclusion, we report a simple method for mitigating cytotoxicity of GQDs. By encapsulating well-defined GQDs in a PEG nanoparticle, we greatly reduce their cytotoxicity. We attribute the unprecedented low cytotoxicity to the ability of PEGylated GQDs to produce less intracellular ROS. The strategy employed here thus offers a platform for developing theranostic probes and will help in expanding the use of GQDs in biomedicine.

■ ASSOCIATED CONTENT

Supporting Information

Detailed experimental procedures and supplementary Figures S1−S13. This material is available free of charge via the Internet at http://pubs.acs.org.

■ AUTHOR INFORMATION

Corresponding Author

*E-mail: sneetu@iitd.ac.in. Tel.: + 91-011-26591422.

Author Contributions

§These authors contributed equally (A.C. and S.D.).

Notes

The authors declare no competing financial interest.

■ ACKNOWLEDGMENTS

Financial support from CSIR-NCL is gratefully acknowledged. N.S. acknowledges funding from DST-Nanomission and IYBA (DBT). A.C. and S.D. thank UGC, and D.B.S. thanks CSIR for fellowship. We thank NCL and IIT-Delhi for characterization facilities.

■ REFERENCES

(1) Shen, J.; Zhu, Y.; Yang, X.; Li, C. *Chem. Commun.* **2012**, *48*, 3686−3699.
(2) Zhu, S.; Tang, S.; Zhang, J.; Yang, B. *Chem. Commun.* **2012**, *48*, 4527−4539.
(3) Li, L.; Wu, G.; Yang, G.; Peng, J.; Zhao, J.; Zhu, J.-J. *Nanoscale* **2013**, *5*, 4015−4039.
(4) Wu, Z. L.; Gao, M. X.; Wang, T. T.; Wan, X. Y.; Zheng, L. L.; Huang, C. Z. *Nanoscale* **2014**, *6*, 3868−3874.
(5) Ristic, B. Z.; Milenkovic, M. M.; Dakic, I. R.; Todorovic-Markovic, B. M.; Milosavljevic, M. S.; Budimir, M. D.; Paunovic, V. G.; Dramicanin, M. D.; Markovic, Z. M.; Trajkovic, V. S. *Biomaterials* **2014**, *35*, 4428−4435.
(6) Liu, Z.; Robinson, J. T.; Sun, X.; Dai, H. *J. Am. Chem. Soc.* **2008**, *130*, 10876−10877.
(7) Wang, C.; Wu, C.; Zhou, X.; Han, T.; Xin, X.; Wu, J.; Zhang, J.; Guo, S. *Sci. Rep.* **2013**, *3*, 2852.
(8) Zhu, S.; Zhang, J.; Qiao, C.; Tang, S.; Li, Y.; Yuan, W.; Li, B.; Tian, L.; Liu, F.; Hu, R.; Gao, H.; Wei, H.; Zhang, H.; Sun, H.; Yang, B. *Chem. Commun.* **2011**, *47*, 6858−6860.
(9) Chang, Y.; Yang, S.-T.; Liu, J.-H.; Dong, E.; Wang, Y.; Cao, A.; Liu, Y.; Wang, H. *Toxicol. Lett.* **2011**, *200*, 201−210.
(10) Qu, G.; Wang, X.; Wang, Z.; Liu, S.; Jiang, G. *Nanoscale Res. Lett.* **2013**, *8*, 198.
(11) Akhavan, O.; Ghaderi, E.; Akhavan, A. *Biomaterials* **2012**, *33*, 8017−8025.
(12) Liao, K.-H.; Lin, Y.-S.; Macosko, C. W.; Haynes, C. L. *ACS Appl. Mater. Interfaces* **2011**, *3*, 2607−2615.
(13) Sun, Y.; Wang, S.; Li, C.; Luo, P.; Tao, L.; Wei, Y.; Shi, G. *Phys. Chem. Chem. Phys.* **2013**, *15*, 9907−9913.
(14) Peng, J.; Gao, W.; Gupta, B. K.; Liu, Z.; Romero-Aburto, R.; Ge, L.; Song, L.; Alemany, L. B.; Zhan, X.; Gao, G.; Vithayathil, S. A.; Kaipparettu, B. A.; Marti, A. A.; Hayashi, T.; Zhu, J.-J.; Ajayan, P. M. *Nano Lett.* **2012**, *12*, 844−849.
(15) Chong, Y.; Ma, Y.; Shen, H.; Tu, X.; Zhou, X.; Xu, J.; Dai, J.; Fan, S.; Zhang, Z. *Biomaterials* **2014**, *35*, 5041−5048.
(16) Bhunia, S. K.; Saha, A.; Maity, A. R.; Ray, S. C.; Jana, N. R. *Sci. Rep.* **2013**, *3*, 1473.
(17) Zhang, W.; Guo, Z.; Huang, D.; Liu, Z.; Guo, X.; Zhong, H. *Biomaterials* **2011**, *32*, 8555−8561.
(18) Zhang, L.; Xia, J.; Zhao, Q.; Liu, L.; Zhang, Z. *Small* **2010**, *6*, 537−544.
(19) Sun, X.; Liu, Z.; Welsher, K.; Robinson, J. T.; Goodwin, A.; Zaric, S.; Dai, H. *Nano Res.* **2008**, *1*, 203−212.
(20) Shang, L.; Nienhaus, K.; Nienhaus, G. U. *J. Nanobiotechnol.* **2014**, *12*, 5.
(21) Chen, S.; Liu, J.-W.; Chen, M.-L.; Chen, X.-W.; Wang, J.-H. *Chem. Commun.* **2012**, *48*, 7637−7639.
(22) Pan, D.; Zhang, J.; Li, Z.; Wu, M. *Adv. Mater.* **2010**, *22*, 734−738.
(23) Gollavelli, G.; Ling, Y.-C. *Biomaterials* **2012**, *33*, 2532−2545.
(24) Shinde, D. B.; Pillai, V. K. *Chem.—Eur. J.* **2012**, *18*, 12522−12528.
(25) Shen, J.; Zhu, Y.; Yang, X.; Zong, J.; Zhang, J.; Li, C. *New J. Chem.* **2012**, *36*, 97−101.
(26) Pu, Y.; Hu, F.; Huang, F.; Davison, B. H.; Ragauskas, A. J. *Biotechnol. Biofuels* **2013**, *6*, 15.
(27) Moxley, G.; Gaspar, A. R.; Higgins, D.; Xu, H. *J. Ind. Microbiol. Biotechnol.* **2012**, *39*, 1289−1299.
(28) Zhang, X.; Wang, S.; Liu, M.; Yang, B.; Feng, L.; Ji, Y.; Tao, L.; Wei, Y. *Phys. Chem. Chem. Phys.* **2013**, *15*, 19013−19018.
(29) Shen, J.; Zhu, Y.; Chen, C.; Yang, X.; Li, C. *Chem. Commun.* **2011**, *47*, 2580−2582.
(30) Guo, Y.; Deng, L.; Li, J.; Guo, S.; Wang, E.; Dong, S. *ACS Nano* **2011**, *5*, 1282−1290.
(31) Song, Y.; Wang, X.; Zhao, C.; Qu, K.; Ren, J.; Qu, X. *Chem.—Eur. J.* **2010**, *16*, 3617−3621.
(32) Wu, X.; Tian, F.; Wang, W.; Chen, J.; Wu, M.; Zhao, J. X. *J. Mater. Chem. C* **2013**, *1*, 4676−4684.
(33) Foucaud, L.; Wilson, M. R.; Brown, D. M.; Stone, V. *Toxicol. Lett.* **2007**, *174*, 1−9.